

# Absorption of finite amplitude focused ultrasound

Diane Dalecki, Edwin L. Carstensen, and Kevin J. Parker

*Department of Electrical Engineering and the Rochester Center for Biomedical Ultrasound, University of Rochester, Rochester, New York 14627*

David R. Bacon

*Division of Radiation Science and Acoustics, National Physical Laboratory, Teddington, Middlesex TW11 0LW, United Kingdom*

(Received 4 August 1990; accepted for publication 6 December 1990)

Predictions of the absorption of focused finite amplitude waves based on weak shock theory have been tested experimentally. The characteristics of this absorption are qualitatively different from those associated with small signal losses. Under appropriate conditions, the absorption of finite amplitude ultrasound is determined largely by source amplitude, field geometry, and the nonlinear properties of the medium and is only weakly dependent upon the small signal absorption coefficient of the material. These effects are seen most dramatically in sharply focused sound fields. To emphasize nonlinear absorption in an experimental test of these predictions, measurements of heating were made in agar which has a very small linear absorption coefficient. Under appropriate conditions, nonlinear losses can make the effective absorption coefficient of this poorly absorbing material somewhat greater than the soft tissues of the body.

PACS numbers: 43.80.Cs, 43.25.Ed, 43.35.Bf

## INTRODUCTION

In a homogeneous medium at small signal levels, it is possible to characterize the losses of ultrasound and the consequent generation of heat by a single property of the propagating medium which we call the absorption coefficient. However, propagation at finite amplitudes leads to waveform distortion and to increased absorption. At a critical combination of distance and amplitude, a pressure discontinuity develops and there is subsequently a continuous process of shock formation and decay with excess absorption associated uniquely with the shock front. It is possible to define an absorption *parameter* to relate the local energy loss to the local intensity but it is much more complex than the absorption *coefficient* because it depends upon the geometry of the sound field, the distance traveled, and the nonlinear properties of the medium (Carstensen *et al.*, 1982; Swindell, 1985, 1986).

Blackstock's (1966) "weak shock" theory<sup>1</sup> provides insight into these processes. [Note that "weak," in this context, simply means that the particle velocity is much less than the sound speed. All medically interesting sound fields, including those used in lithotripsy, are "weak" by this definition.] The theory assumes that linear absorption is negligible and that losses occur only at the pressure discontinuity in the wave front and depend only upon the degree of shock formation. These losses occur as a result of strong irreversible processes generally resulting from the accentuated influences of viscosity, heat conduction, and relaxation at the discontinuity and depend upon the strength of the shock and the shape of the waveform on either side of the shock. This "weak shock absorption  $\alpha_{ws}$ " is essentially independent of the magnitude of the linear absorption coefficient of the medium as long as the linear absorption is small.

Guided by weak shock theory, we have contrived an

experimental arrangement which demonstrates the interesting characteristics of  $\alpha_{ws}$ . First, because sharply focused fields yield the largest values of  $\alpha_{ws}$ , we have used focused sound to emphasize finite amplitude absorption as opposed to linear losses. Second, for the propagating medium, we chose water which has the lowest linear absorption coefficient of any useful material. Third, we used a thermocouple to obtain a direct measurement of the conversion of acoustic to thermal energy. To avoid convection heat loss at the thermocouple, it was embedded in agar, which itself has a low, but non-negligible, linear absorption coefficient. This required that we deal with another specialized aspect of nonlinear absorption—the modification in the absorption which occurs when a shock wave seeks a new equilibrium distribution of harmonic components after passing from one medium into another with different acoustical properties. The excess losses that occur near the interface in the more highly absorbing medium are of interest in certain applications of ultrasound in obstetrics where a poorly absorbing fluid medium separates the source transducer from the fetus.

In our experiments, a focused sound wave propagated through water, developing a shock and suffering excess absorption from finite amplitude effects along the way. Upon entering the agar, this weak shock absorption continued and produced heat at the thermocouple. In addition to the weak shock absorption, there was heating of the agar simply because of its linear properties. This heating provides a low amplitude floor for the effective absorption parameter of the material. Even if the process of wave distortion associated with the nonlinear properties of the medium ceased as soon as the wave entered the agar, there would be an additional excess loss over the linear value simply because the incident wave contains a rich spectrum of harmonic components. The presence of these harmonics alone, even without the continued distortion of the wave by nonlinear processes, can

lead to an increase in the effective absorption coefficient of the material by as much as a factor of 2 for a short distance after the wave enters the agar. We have called this phenomenon *material absorption*  $\alpha_{\text{mat}}$  to differentiate it from the weak shock absorption which, in the limiting case, is independent of the linear absorption coefficient of the material.<sup>2</sup> [In an earlier study (Carstensen *et al.*, 1982), we used the term “harmonic absorption parameter” for  $\alpha_{\text{mat}}$  and  $\alpha_{\text{ws}}$  was called “the finite amplitude absorption parameter.”] Our experimental design attempted to emphasize  $\alpha_{\text{ws}}$  by minimizing  $\alpha_{\text{mat}}$ . Thus, in our simplified view of the phenomena, there are two qualitatively different kinds of absorption taking place in the material. One,  $\alpha_{\text{ws}}$ , depends almost entirely upon the characteristics of the sound field while the other,  $\alpha_{\text{mat}}$ , depends upon the linear absorption properties of the medium. In both processes, losses result from the generation and absorption of harmonic frequencies of the propagating wave. However, in the first case, the rate of generation and loss of this high frequency energy is independent of the linear absorption coefficient of the medium. To calculate  $\alpha_{\text{ws}}$ , one may use weak shock theory. This describes the limiting behavior of a stable shock for small absorption coefficients (Taylor, 1910; Lighthill, 1956). The Taylor shock represents a balance between nonlinear effects and the influence of absorption, but when a new medium is entered, this balance no longer holds. Consequently, the overall absorption upon entering a new medium could be greater (or less) than before. The theoretical treatment described here gives an estimate of the change in absorption when this balance is being re-established and should therefore be valid close to the surface of the agar.

### I. THEORY

When sound propagation becomes nonlinear, losses are no longer proportional to intensity and the effective absorption parameter  $\alpha$  has meaning only in the basic definition

$$\alpha = -\frac{\nabla \cdot \mathbf{I}}{2I}, \quad (1)$$

where  $\mathbf{I}$  is the local intensity vector and  $I$  is its modulus. For a plane wave, the local intensity is written as

$$\mathbf{I}(z) = \mathbf{e}_z I_0 \sum_{n=1}^{\infty} B_n^2(\sigma), \quad (2)$$

where  $\mathbf{e}_z$  is the unit vector in the direction of propagation and the harmonic amplitudes  $B_n(\sigma)$  are defined below. For an ideal, spherically converging wave (Blackstock, 1966, 1972),

$$\mathbf{I}(z) = \mathbf{e}_z I_0 \sum_{n=1}^{\infty} B_n^2(\sigma), \quad (2)$$

where  $z_0$  is the focal distance,  $z_r$  is the distance from the focus, and  $\mathbf{e}_z$  is the unit vector in the direction of propagation (Fig. 1). This simple model [Eq. (3)], and equations derived under its assumption, cannot be accurately applied at the focus because the wave amplitude becomes infinite. It also has limited application elsewhere in the beam because it is a one-dimensional model and does not take account of diffraction. Some of these problems can be overcome by using a Gaussian beam profile to model the radial dependence

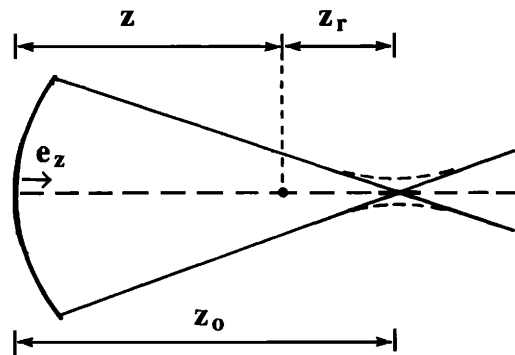


FIG. 1. Idealized focusing geometry. Using a source with a focal length  $z_0$ , a sample is placed at the position  $z$  from the source and  $z_r$  from the focus. The spherically converging model assumes a point focus. In reality, diffraction yields a finite beam width at the focus.

of the wave amplitude (Bacon, 1986). The Gaussian model can be used to predict the nonlinear field in the focal region of a focused piston source, by appropriate matching of the experimental conditions to the theory (Bacon, 1986). This model does not describe the full near-field structure of a piston source, but it does give an approximate description of the spatial variation of intensity in the focal region. Applying the model to determine the intensity gives (see the Appendix)

$$\begin{aligned} I(z,r) = I_0 G^2 e^{[-2r^2/a^2(1+R^2)]} & \left( \frac{rR}{r_0(1+R^2)^2} \mathbf{e}_r \right. \\ & \left. + \frac{1}{(1+R^2)} \mathbf{e}_z \right) \sum_{n=1}^{\infty} B_n^2[\sigma(z,r)], \end{aligned} \quad (4)$$

where  $\mathbf{e}_z$  is the unit vector directed along the axis of a cylindrical coordinate system centered on the focus and  $\mathbf{e}_r$  is the unit vector in the radial direction.  $G$  is the focal amplitude gain for the experimental sound field,  $R = -(z_r/z_0)(G_f^2 - 1)^{1/2}$ ,  $r$  is the radial position,  $a$  is the focal beam radius at the  $\exp(-1)$  amplitude level,  $r_0 = ka^2/2$ ,  $k$  being the wavenumber  $2\pi/\lambda$ , where  $\lambda$  is the wavelength of the sound, and  $G_f = d/a$  is the theoretical focal gain for a Gaussian beam where  $d$  is the radius of the transducer. For our computations, the experimentally measured focal amplitude gain was used for both  $G$  and  $G_f$ . The focal gain was equal to the square root of the ratio of the measured focal intensity to the measured source intensity. On the axis of the focused sound field, the intensity becomes

$$I(z,0) = I_0 G^2 \left( \frac{1}{1+R^2} \mathbf{e}_z \right) \sum_{n=1}^{\infty} B_n^2(\sigma). \quad (5)$$

The harmonic coefficients  $B_n$  given by Blackstock (1966) are

$$B_n = \frac{2}{n\pi\sigma} \left( \phi_{\min} + \int_{\phi_{\min}}^{\pi} \cos n(\phi - \sigma \sin \phi) d\phi \right), \quad (6)$$

where  $\phi_{\min}$  is given by the transcendental relation

$$\begin{aligned} \phi_{\min} &= \sigma \sin \phi_{\min} \quad \text{for } 1 < \sigma \\ \phi_{\min} &= 0 \quad \text{for } \sigma < 1: \end{aligned} \quad (7)$$

The waveform at the source,  $z_r = z_0$ , is assumed to be sinusoidal, i.e., at the source,  $B_n = 1$  for  $n = 1$ , and  $B_n = 0$  for  $n \neq 1$ . The shock parameter  $\sigma$  in these expressions increases

as the wave progresses and for media with low linear absorption coefficients, serves as a descriptor of the degree of finite amplitude distortion.<sup>3</sup> [For  $\sigma < 1$ , there are no discontinuities in the wave but the waveform may be distorted. For this reason,  $\sigma$  is sometimes called the distortion parameter.] In its general form, the shock parameter is given by the line integral along the path  $l$  [ray tube, (Blackstock, 1972)] as follows:

$$\sigma = \beta k \int \epsilon(l) dl, \quad (8)$$

where  $\beta$  is the nonlinearity parameter of the medium,

$$\epsilon = u/c_0 \quad (9)$$

is the acoustic Mach number, where  $u$  is the particle velocity amplitude, and  $c_0$  is the small amplitude sound speed in the medium. At the source,

$$\epsilon_0 = u_0/c_0 = [2I_0/\rho c_0^3]^{1/2},$$

where  $u_0$  is the source particle velocity amplitude,  $\rho$  is the density of the medium, and  $I_0$  is the source intensity. For plane waves,  $\epsilon$  is constant and (Blackstock, 1966)

$$\sigma = \beta \epsilon_0 k z, \quad (10)$$

for spherically converging waves  $\epsilon = e_z(\epsilon_0/z_r)$  and (Blackstock, 1972),

$$\sigma = \beta \epsilon_0 k z_0 \ln(z_0/z_r), \quad (11)$$

and for a focused Gaussian beam  $\epsilon = [\epsilon_0 G_f(1 + R^2)^{-1/2}]$  for a path along the axis and, so (Bacon, 1986),

$$\sigma = \frac{\beta \epsilon_0 k z_0 G_f}{\sqrt{G_f^2 - 1}} \{ \ln [ G_f + \sqrt{G_f^2 - 1} ] + \ln [ R + \sqrt{1 + R^2} ] \}. \quad (12)$$

The Appendix gives the off-axis formulation of the shock parameter. For the field on the acoustic axis the spherically converging wave model [Eq. (3)] and the focused wave model [Eq. (5)] are similar except near the origin (focus). Note that for  $z_r \sim z_0 \rightarrow \infty$ , Eqs. (11) and (12) approach the plane-wave case where  $z_0 = z_r = z$ .

### A. Weak shock absorption

Equation (1) can be applied to Eqs. (2)–(5) to obtain a *weak shock absorption parameter*  $\alpha_{ws}$  based on weak shock theory. Each of Eqs. (2)–(5) can be expressed in the form

$$I(z,r) = I_1(z,r) \sum B_n^2[\sigma(z,r)], \quad (13)$$

where  $\sigma$  is defined according to Eq. (8). In each expression for the intensity of the above form, the contribution to the divergence from  $I_1$  is zero since it represents the linear, lossless limit. Hence,

$$\nabla \cdot I(z,r) = I_1(z,r) \cdot \nabla [\sigma(z,r)] \frac{\partial}{\partial \sigma} \sum B_n^2(\sigma). \quad (14)$$

Now, since  $\sigma$  is defined as an integral along a ray tube (which is by definition parallel to  $I$ ),  $I_1 \cdot \nabla [\sigma] = |I_1| |\nabla [\sigma]|$ , hence, from Eq. (1)

$$\alpha_{ws} = - \frac{1}{\sigma} \frac{\partial \sigma}{\partial l} \frac{\sigma(\partial/\partial \sigma) \sum B_n^2(\sigma)}{2 \sum B_n^2(\sigma)}. \quad (15)$$

Thus, the expression for  $\alpha_{ws}$  can be separated into a purely geometrical factor which depends upon the convergence of the sound field [Eq. (8)]

$$F^{-1} = \frac{1}{\sigma} \frac{\partial \sigma}{\partial l} = \frac{\epsilon(l)}{\int \epsilon(l) dl}, \quad (16)$$

and a part which can be determined generally, since it is just a function of  $\sigma$  and is determined by weak shock theory [right-hand side of Eq. (17)]

$$\alpha_{ws} F = - \frac{\sigma(\partial/\partial \sigma) [\sum B_n^2(\sigma)]}{2 \sum B_n^2(\sigma)}. \quad (17)$$

The expression on the right-hand side of Eq. (17) has been evaluated using the time-domain solution to the finite amplitude absorption problem (Blackstock, 1966, 1990)

$$\alpha_{ws} F = \frac{2\phi_{\min}^3}{2\phi_{\min}^3 + 3\sigma\phi_{\min} \cos(\phi_{\min}) + 3(\pi - \phi_{\min})\sigma^2}, \quad (18)$$

where  $\phi_{\min}$  is as given in Eq. (7). For a plane wave,

$$F = z, \quad (19)$$

for a spherically converging wave,

$$F = z_r \ln(z_0/z_r) \quad (20)$$

and, on the axis of a focused Gaussian beam (see the Appendix)

$$F = \frac{z_0 \sqrt{1 + R^2}}{\sqrt{G_f^2 - 1}} \{ \ln [ G_f + \sqrt{G_f^2 - 1} ] + \ln [ R + \sqrt{1 + R^2} ] \}. \quad (21)$$

The right-hand side of Eq. (17) is completely determined by the shock parameter  $\sigma$ . Hence, it provides us with a relationship (Fig. 2) which can be used to determine  $\alpha_{ws}$  as a function of  $\sigma$ . As we can see from Fig. 2,  $\alpha_{ws}$  is characterized by: (1) a zero value for  $\sigma < 1$ , (2) a very rapid increase in the range  $1 < \sigma < 2$ , and (3) an upper limit,  $\alpha_{ws} = F^{-1}$ , for  $\sigma \gg 1$  which depends only on geometrical parameters. Comparison of the behavior of the function  $F$  for plane, spherically converging, and focused waves is given in Fig. 3. Note that

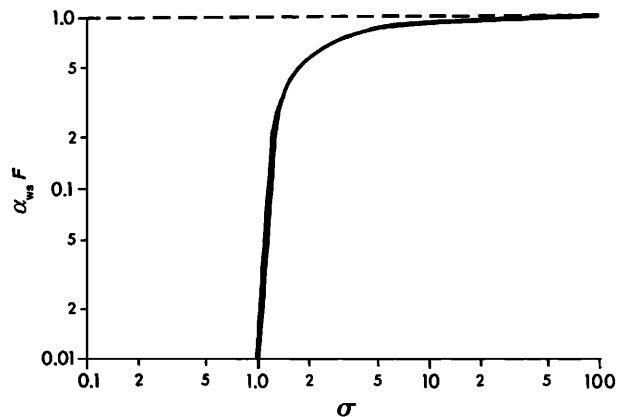


FIG. 2. The weak shock absorption parameter  $\alpha_{ws}$  plotted as a function of the shock parameter  $\sigma$ . The parameter  $F$  (Fig. 3) depends only on geometrical factors of the sound field.

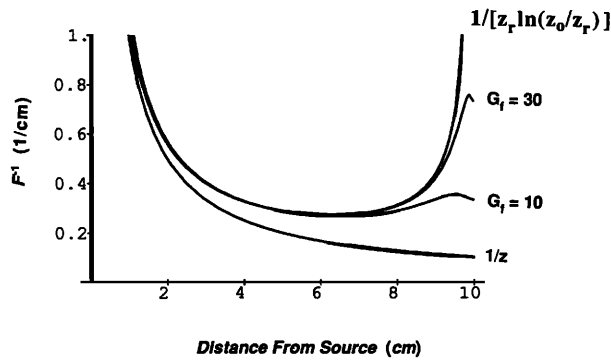


FIG. 3. Limiting (large  $\sigma$ ) values of the weak shock absorption parameter  $\alpha_{ws}$ . The reciprocal of  $F$  [Eqs. (19)–(21)] is plotted as a function of propagation distance from the source for (1) a plane wave ( $1/z$ ), (2) a spherically converging wave [ $1/(z_r \ln z_0/z_r)$ ], and (3) focused waves [Eq. (21)] with focal amplitude gains of 10 and 30. In this example the focus is located at 10 cm from the source. Note the agreement between focused waves and spherically converging waves except very near the focus.

the maximum value for  $F^{-1}$  for plane waves is near the source whereas, in converging and focused waves, large values for  $F^{-1}$  occur near the focus as well. For the focused Gaussian beam, the maximum value of  $F^{-1}$  occurs just before the focus at an approximate distance of  $z_0 \{1 - 1/[\ln(G_f + \sqrt{G_f^2 - 1})\sqrt{G_f^2 - 1}]\}$  from the source when  $G_f \gg 1$ .

For conditions of interest to biomedical ultrasound, e.g.,  $z = 5$  to 10 cm, the maximum value of  $\alpha_{ws}$ , in the plane-wave case, may be of the order of 0.1 to 0.2 Np/cm. In contrast, Figs. 2 and 3 show that, with focused sound beams (e.g., with  $z_r = 0$  and  $z_0 = 10$  cm,  $G_f = 30$ ), it is possible to achieve values of  $\alpha_{ws}$  greater than 0.5 Np/cm, a value somewhat greater than the linear absorption coefficients of most soft tissues. Thus in principle, finite amplitude absorption in focused sound fields can be much larger than is found in plane wave fields.

At first glance, the fact that  $\alpha_{ws}$  becomes independent of source amplitude for  $\sigma \gg 3$  might suggest that the heating rate would be directly proportional to the output of the source at large source intensities  $I_0$ . However, it should be noted that the absorption parameter is defined in terms of the local intensity [Eq. (1)], and the local intensity also approaches a constant value at large  $I_0$  (saturation). Hence, the heating rate approaches a constant value independent of the source intensity at large  $I_0$ .

The losses described by Eq. (17) are completely foreign to the concepts of linear acoustics. Weak shock theory (Blackstock, 1966) assumes that losses in the medium arising from the fundamental frequency, linear absorption coefficient of the medium  $\alpha_1$  are small. As long as this assumption is valid,  $\alpha_{ws}$  is independent of the linear loss mechanisms of the material. In reality, the losses represented by  $\alpha_{ws}$  occur because of generation and absorption of high frequencies during shock development. However, the degree to which these losses occur depends only upon the shock and not upon the specific details of the loss mechanisms involved. Thus operationally,  $\alpha_{ws}$  is a qualitatively different loss mechanism and has a fundamentally different depend-

ence on propagation distance, frequency, and material properties from the dependence observed under linear propagation conditions. Specific examples of  $\alpha_{ws}$  are given at the end of this section.

## B. Absorption in the experimental medium

Weak shock losses are adequate to describe the absorption of the medium as long as its linear absorption coefficient  $\alpha_1$  at the fundamental frequency is small, i.e., when  $\alpha_1 \ll 1/F$ . For water, this is true for most of the conditions used in this study. For other materials, there are small-signal losses which must be included if we are to describe heating adequately, particularly close to the interface between two media as explained in the Introduction.

In the region of applicability of weak shock theory, a balanced distribution of harmonics develops so that attenuation occurs at the rate given by Eq. (17). The precise distribution of harmonics which produces that rate of loss will depend upon the frequency-dependent linear absorption coefficient of the medium. In a medium with small but different absorption properties, a different distribution would develop, yielding the same attenuation. Upon transmission from one medium to another with small but different absorption properties, the wave must travel a certain distance before the distribution of harmonics reaches the new equilibrium for the new medium. In that short transition distance, the net absorption could be higher or lower than given by Eq. (17).

Of course, this is not the whole story for any real propagating medium. At low amplitudes, the absorption does not go to zero but rather has the value of the linear absorption coefficient  $\alpha_1$  of the material. Furthermore, even for  $\sigma < 1$ , nonlinearities of the propagating medium transfer energy from the fundamental frequency of the wave to higher order harmonics that are absorbed at a higher rate than the fundamental by linear loss mechanisms in the medium. These losses can be determined, first, by computing the harmonic spectrum at a particular point along the propagation path using weak shock theory and then by allowing the wave to propagate an infinitesimal distance  $\Delta l$  along a ray tube, taking into account the nonzero absorption of the material, i.e.,

$$I(\Delta l) = e_z I_0 \sum_{n=1}^{\infty} B_n^2(\sigma) e^{-2\alpha_n \Delta l}, \quad (22)$$

where  $\alpha_n$  is the linear absorption coefficient of the material at the  $n$ th harmonic of the source frequency. Substituting this in Eq. (1) gives the total *finite amplitude absorption parameter*  $\alpha_{fin}$  (as  $\Delta l$  approaches zero)

$$\alpha_{fin}(\sigma) = \frac{\sum \alpha_n B_n^2(\sigma)}{\sum B_n^2(\sigma)} + \alpha_{ws} = \alpha_{mat} + \alpha_{ws}. \quad (23)$$

The first term is the *material absorption parameter*  $\alpha_{mat}$ . It takes care of linear losses and modifications in those losses resulting from changes in the waveform through nonlinear processes. The second term expresses the losses at the shock front as given by Eq. (17). For  $\sigma < 1$ ,  $\alpha_{ws} = 0$  and the total finite amplitude absorption is just  $\alpha_{mat}$ . Furthermore, since the waveform is not greatly distorted for  $\sigma < 1$ , a good approximation to the total absorption can be obtained by sum-

ming over a modest number of harmonics. A number of methods exist for determining the maximum number of harmonics to be used in the summation. For a nonzero propagation distance  $\Delta l$  into the new medium, the maximum harmonic to be used can be estimated by requiring that the exponential term in Eq. (22) be significant.

For  $\sigma > 1$ ,  $\alpha_{ws}$  accounts for the absorption which would occur even if the linear loss of the medium were very small whereas  $\alpha_{mat}$  is a first order attempt to estimate the excess losses arising from nonzero but modest linear absorption in a real medium. This will be valid in a real medium if its linear absorption is small enough that weak shock theory correctly represents the harmonic distribution in the wave. This clearly is true in our experiments at the interface between water and the agar sample. An example of the dependence of  $\alpha_{mat}$  on the shock parameter  $\sigma$  is given in Fig. 4.

The parameter  $\alpha_{mat}$  occurs because the nonzero losses at low frequency are neglected in weak shock theory. It also accounts for the process of achieving a stable shock structure in the new medium. This stabilization occurs over a distance  $\Delta l$ , such that the exponential term in Eq. (22) becomes insignificant, as given by  $\Delta l \alpha_n \cong 1$ . Thus the high frequencies stabilize more rapidly with distance than the low frequencies. For these reasons, the summation used to obtain  $\alpha_{mat}$  should not extend to very high frequencies for nonzero propagation distances. A comparison of the predictions of Eq. (23) with a more rigorous analytical formulation involving the solution of Burgers equation for the plane-wave case (Christopher, 1990 and Christopher and Parker, 1990) shows that this approach [i.e., Eq. (23)] should be reasonably accurate for the experimental conditions used here. The 3% agar used for the experiments had a measured small signal absorption coefficient which was approximately proportional to the frequency in the low megahertz region,

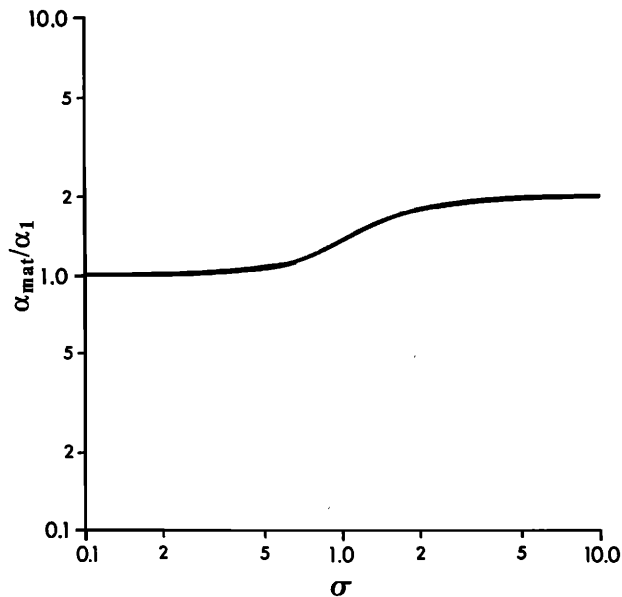


FIG. 4. The material absorption parameter  $\alpha_{mat}$  plotted as a function of the shock parameter  $\sigma$ . It is assumed here that the small signal absorption coefficient of the material is directly proportional to frequency and  $\alpha_{mat}$  is normalized to the linear fundamental absorption coefficient  $\alpha_1$ .

whereas the absorption in water has a quadratic frequency dependence. Hence, there is some frequency  $f_{max}$  where the two absorption coefficients will be equal and this was taken to give the limiting frequency for the summation. This frequency corresponds to a certain harmonic number  $n_{max}$ . Applying Eq. (22) to the case where the wave has traveled a small distance  $l'$  into the medium gives

$$\alpha_{mat}(\sigma) = \frac{\sum_{n=1}^{n_{max}} \alpha_n B_n^2(\sigma)|_{l'=0} e^{-2\alpha_n l'}}{\sum_{n=1}^{n_{max}} B_n^2(\sigma)|_{l'=0} e^{-2\alpha_n l'}}, \quad (24)$$

where  $\alpha_n$  is the linear absorption coefficient of the medium for the  $n$ th harmonic of the fundamental frequency of the sound field. In this study,  $l'$  is small and the wave is assumed to be plane over that distance. For the reasons given above, this model is expected to be valid for a distance into the sample of about  $1/\alpha_{n_{max}}$  which is of the order of 1 cm for the material used in this study.

### C. Tests of theory

Equation (1) indicates that, to measure the absorption parameter, it is necessary to know both the intensity  $I$  and its divergence. With the broad beams of plane piston sources, it is possible to measure total local intensities even at finite amplitudes by using a steel sphere radiometer (Carstensen *et al.*, 1980, 1982). Unfortunately, we had no completely satisfactory way to measure the local intensity in a sharply focused sound field at very high intensities at megahertz frequencies. Hence, the absorption parameter itself [as defined in Eq. (1)] could not be measured directly. However, both the source intensity and the heating rate of a sample could be measured directly. The source intensity  $I_0$  can be determined radiometrically. The heating rate  $H$  in units of absorbed power density at the target is just  $-\nabla \cdot I$  where  $I$  is the local intensity. This heating rate in turn can be related to the rate of change of temperature  $T$

$$\frac{dT}{dt} = \frac{-\nabla \cdot I}{\rho C}, \quad (25)$$

where  $\rho$  is the density and  $C$  is the specific heat of the material. Since the source intensity and the heating rate in the field can be related theoretically [e.g., through Eqs. (4), (17), and (23)] this provides us with an experimental test of the theory.

First, let us consider the predicted influence of the material absorption  $\alpha_{mat}$  on the local heating rate in the field. Figure 5 shows the heating rate  $H$  for this absorption normalized to the source intensity  $I_0$  plotted as a function of source intensity. This is the same process as shown in Fig. 4 except that here all of the quantities are directly measurable. The heating rate depends upon the small-amplitude absorption coefficient (and its dependence upon frequency) and the harmonic composition of the sound field which, in turn, depends upon the source intensity according to Eqs. (3)–(5). A specific example is given in Fig. 5, but the general characteristics of the  $(H/I_0)_{mat}$  curves are all alike. For  $\sigma \ll 1$  (linear acoustics),  $(H/I_0)_{mat}$  is constant and determined by the small signal absorption of the medium at the fundamental frequency. As  $I_0$  increases, the normalized heating rate rises reaching a maximum at approximately

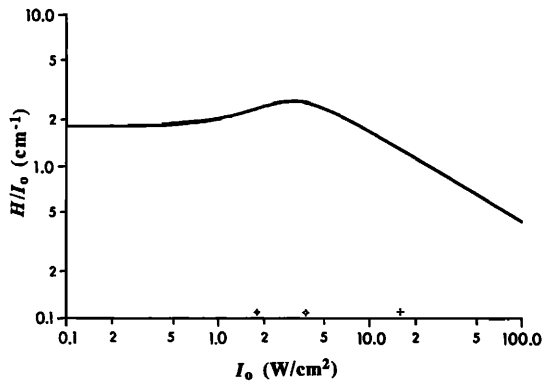


FIG. 5. Predicted heating rate  $H$  resulting from excess material absorption normalized to the source intensity  $I_0$ . Frequency = 4 MHz; observation point is 0.5 cm beyond the surface of a 3% agar sample; focal length of the source = 10 cm; distance of the sample from the focus = 2 cm; measured small signal absorption coefficient is 0.01 Np/cm/MHz.  $n_{\max} = 15$ . ( $\sigma = 1$  at  $\blacklozenge$ ;  $\sigma = 1.5$  at  $\diamond$ ;  $\sigma = 3$  at  $+$ ).

$\sigma = 1.5$  and then falls inversely with  $I_0$  for  $\sigma > 3$ .

Second, consider the characteristics of weak shock heating as it relates source intensity to local heat development. The weak shock heating is zero for  $\sigma < 1$  and then rises rapidly near  $\sigma = 1$ .  $(H/I_0)_{ws}$  reaches a maximum at  $\sigma = 1.93$ . For  $\sigma > 3$ ,  $(H/I_0)_{ws}$  decreases inversely with  $I_0$ . The predicted dependence [Eq. (17)] of the normalized weak shock heating on (1) frequency, (2) proximity to the focus, and (3) focal length of the source is illustrated in Fig. 6(a)–(c). Increasing the frequency decreases the source intensity required to produce a given weak shock heating rate but does not affect the maximum possible rate of heating [Fig. 6(a)]. As one approaches the focus of a given sound field, the maximum normalized heating rate increases and it is possible to achieve that maximum rate at lower source intensities [Fig. 6(b)]. If one maintains a constant ratio  $z_r/z_0$  and varies the focal length of the source  $z_0$ , one finds that higher maximum heating rates can be achieved with short focal lengths; however, somewhat higher source intensities are required to produce maximal heating [Fig. 6(c)]. As mentioned above, an analogous phenomenon is found with plane waves. This is illustrated in Fig. 7. In this case, the upper limit to the heating rate increases as the point of observation approaches the source. In all cases, larger source intensities are required to produce this maximal heating when the point of observation is closer to the source.

It is helpful to consider all of these phenomena in terms of the behavior of the function  $F$  in Eq. (17). Since the term on the right-hand side of Eq. (17) reaches a limit of unity for  $\sigma \gg 3$  (Fig. 2), the maximum value of  $\alpha_{ws}$  for a particular geometry is  $1/F$ . In Fig. 6(a), the geometrical factors and hence  $F$  remain constant and so the maximum normalized heating rate is constant. In Fig. 6(b) and (c), the maximum normalized heating rate changes in accordance with variations in  $F$ . The source intensity for which the maximum normalized heating occurs is determined by the requirement that  $\sigma = 1.93$  [Eqs. (10)–(12)]. This agrees with results obtained by others of heating measurements in artificial tissue (Bacon and Carstensen, 1990). When their data are pre-

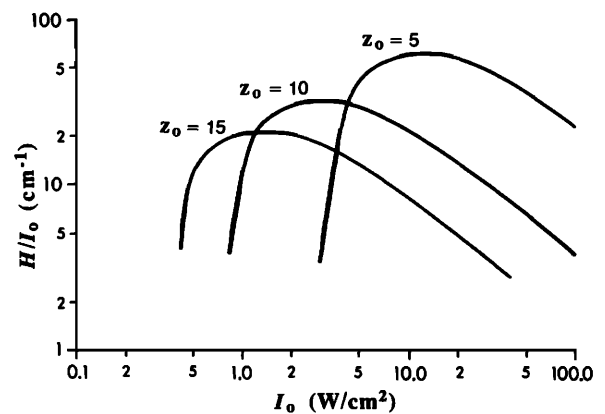
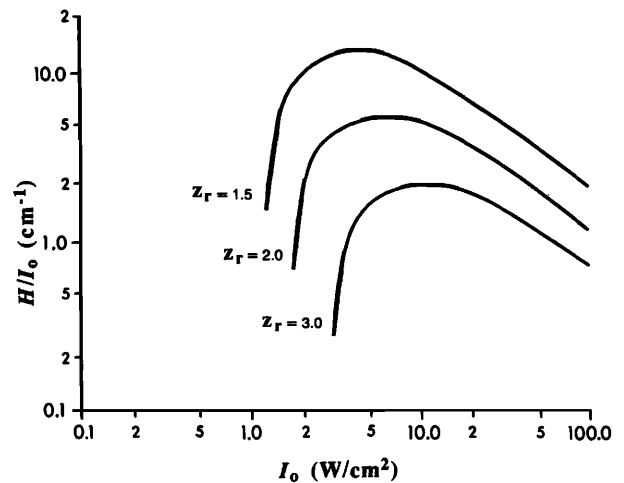
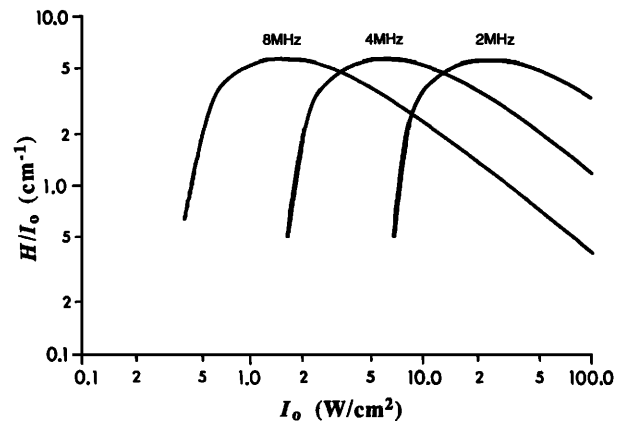


FIG. 6. (a) The effect of frequency on weak shock heating using a spherically converging wave model. For each of the curves,  $z_r = 2$  cm and  $z_0 = 10$  cm. Increasing frequency decreases the intensity required to produce finite amplitude heating but it does not affect the maximum obtainable normalized heating rate  $H/I_0$ . (b) The dependence of weak shock heating on proximity to the focus using a spherically converging wave model. Frequency = 4 MHz;  $z_0 = 10$  cm. The maximum obtainable heating  $H/I_0$  increases as the point of observation approaches the focus and weak shock heating occurs at lower source intensities. Values of  $z_r$  are in cm. (c) The dependence of weak shock heating on the focal length of the source using a spherically converging wave model. Frequency = 4 MHz;  $z_r/z_0 = 0.1$ . For constant ratios, shorter focal lengths produce higher normalized maximum heating rates  $H/I_0$ , but higher source intensities are necessary to achieve maximal heating. Values of  $z_0$  are in cm.

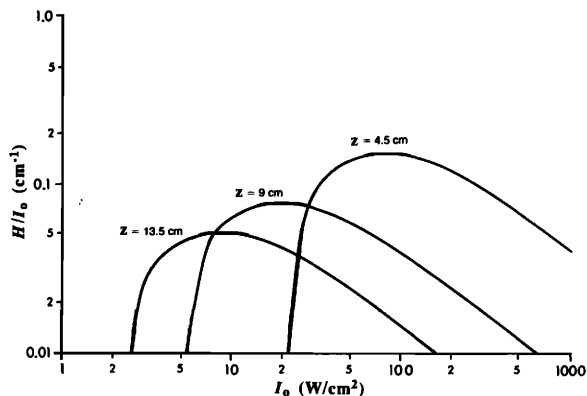


FIG. 7. Normalized weak shock heating for plane waves. Frequency = 4 MHz. Maximum heating rates increase as the point of observation approaches the source but higher source intensities are necessary to achieve maximal heating.

sented as  $H/I_0$ , the maximum heating occurs at approximately  $\sigma = 2$ .

Total heating is the sum of the excess material and weak shock heating rates. This behavior is illustrated in Fig. 8. The assumptions leading to this conclusion should be valid under the experimental conditions of this study.

The approach that we have used here is simple enough to allow a good intuitive feeling for the physical processes that are involved. Weak shock theory provides the basic concepts of finite amplitude absorption. However, it assumes that the linear absorption of the propagating medium is negligible and needs to be applied with care. Separation of absorption into material and weak shock components is a conceptual convenience invoked to deal with the nonzero linear absorption of the medium used for temperature measurements in this study. Equation (5) further adapts the model so that the field has the experimentally observed gain at the focus. With these procedures, it is possible to predict the nonlinear absorption under the special conditions used in this study.

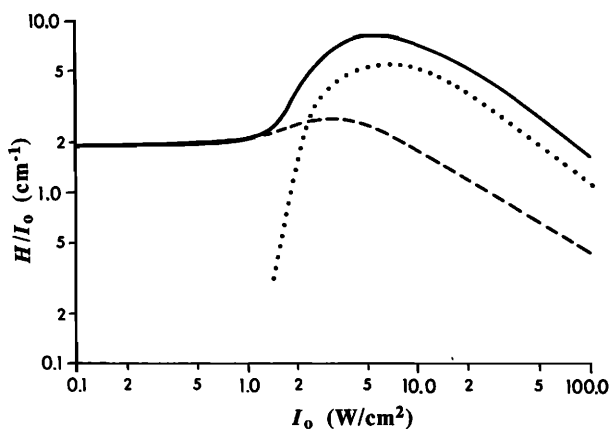


FIG. 8. Total normalized heating rate (—) is assumed to be the sum of the weak shock (···) and material (---) heating contributions. Conditions are as used in Fig. 5.

## II. EXPERIMENTAL PROCEDURES

### A. Source intensity

Focused sound fields were generated by one inch diameter piezoceramic disks (and, in one case, a 2-in. diameter quartz element) which were coupled to planoconcave aluminum lenses. The source intensity  $I_0$  was measured by placing a large absorbing target directly in front of the lens and determining the total acoustic power with a radiation force balance.  $I_0$  was taken to be the total acoustic power divided by the area of the source element in the transducer. The entire system from the input of the power amplifier to the acoustic power in the water immediately in front of the transducer was found to be linear up to the highest powers used in the study. To avoid excessive heating of the sample, only modest average total powers (of the order of 1 W) were used. When finite amplitude effects were desired, the source was pulsed with 100- $\mu$ s on-times and appropriate off-times to keep the heating rates at manageable levels.

### B. Field intensity

At low intensities, our standard probe was a 50- $\mu$ m thermocouple embedded in castable rubber. Using its response to very short bursts ( $< 0.1$  s) of sound, the fine thermocouple is able to resolve the focal beam profiles of all of the transducers used in this study. In those cases in which it was necessary to have absolute values for the field intensity near the focus, we calibrated the response of the thermocouple probe to 0.05-s pulses of sound by comparison with a steel sphere radiometer in an unfocused sound field. Of course, absolute values of intensity in these sound fields were determined only at small amplitudes where the response of the thermocouple is a linear function of intensity.

### C. Sample preparation

To emphasize finite amplitude heating, we sought a solid medium with a very low, small-signal absorption coefficient. In our studies, aqueous preparations of agar served that function. A fine copper-constantan thermocouple (junction diameter  $< 50$   $\mu$ m) was mounted in the sample chamber, 3% agar was poured around the thermocouple and allowed to harden. The distance from thermocouple junction to the front face of the sample was approximately 5 mm. The agar concentration was a compromise between the desired low, small-signal absorption coefficient (which would have been achieved best at low concentrations of agar) and stability and reproducibility of measurements, which required a comparatively solid support for the thermocouple.

### D. Heating measurements

As has been recognized from the first applications of thermocouples for ultrasonic heating measurements (Fry and Fry, 1954), the presence of the thermocouple in the sound field results in localized viscous heating which is a potential source of error. This is particularly troublesome when the inherent absorption coefficient of the medium is very small. Our solution to this problem was to use long exposure times ( $\sim 2$  s). Localized heating of the thermocou-

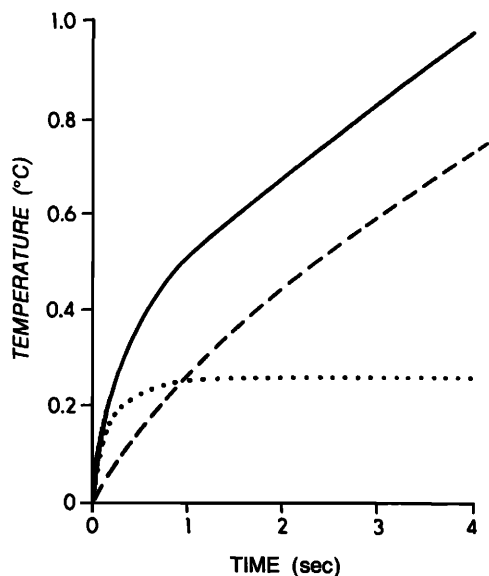


FIG. 9. Representative temperature measurements. The solid curve represents the temperature as recorded by a thermocouple embedded in an agar sample. The dashed curve is the temperature rise which would have occurred in the medium in the absence of the thermocouple. It was obtained by computing a series of heating curves for the measured beam pattern of the source and matching them to the experimental curve in the time period  $t > 1$  s. The dotted curve, the difference between the solid and dashed curves, is the temperature rise which results from localized heating and other spurious effects related to the presence of the thermocouple.

ple is confined to a layer of a few tens of micrometers and, because of heat diffusion, the rate of rise of temperature resulting from localized heating becomes negligible after a few tenths of a second (Fig. 9). In contrast, the direct heating of the medium by absorption, is distributed over the sound beam with a radius of the order of 1 mm. Thus the rate of rise of temperature of the medium between 1 and 2 s is dominated by heating of the medium. Use of the data obtained between 1 and 2 s avoided the artifact of localized heating caused by the presence of the thermocouple in the sound field, but for our focused sound fields, heat diffusion from the beam had a significant effect upon the rate of rise of temperature at times greater than 0.5 s. Hence, it was necessary to apply a theoretical correction to the temperature data (as discussed below) for heat diffusion from the sound beam to obtain the actual heating rate.

For temperature data acquisition, the output of the thermocouple amplifier was recorded on a strip chart or converted to digital form and stored in a laboratory computer. Sample temperature data are shown in Fig. 9. These raw data include contributions from localized relative motion heating of the thermocouple as well as direct heating of the medium. Note the rapid rise in the first 0.1–0.2 s (localized heating) followed by a slower rise which is dominated by heating of the medium. The problem of relative motion losses in a finite amplitude wave has not been investigated. For the present study, the question has been avoided by elimination of local heating from the total heating rates. A further potential source of error is the conduction of heat away from the center of the field along the thermocouple wires. The magnitude of this effect is difficult to estimate, particularly in the dy-

amic system considered here, but an estimate based on the formulation of Dickinson (1985) gave the error to be typically 20% at low amplitudes. Experimental comparisons of the heating rate measured by thermocouples made from different thicknesses of wire indicate that this error is less than 10% in practice.

### E. Beam patterns versus heating patterns

In order to make the corrections to the temperature data for heat diffusion alluded to above, we require information on the spatial distribution of the heating rate at the site of the thermocouple. The only device available to us with adequate resolution for these sharply focused sound fields is the thermocouple itself. At low intensities, we found that the response of the thermocouple to short (0.05 s) pulses was a linear function of local intensity over a range greater than a factor of 10. Thus the low intensity beam patterns could be obtained by slowly sweeping the thermocouple across the beam while pulsing the source at a cycle of 0.05 s on and 2 s off. The focal length  $z_0$  of the field was taken to be the distance from the source where the sound beam had its smallest cross section. At the present time, there is no established way to measure directly the heating patterns of focused sound fields under nonlinear conditions. Thermocouples have sufficient spatial resolution for the task if very short pulses of sound are used in the measurements but we have no basis in present knowledge to conclude that the localized heating at the thermocouple interface is proportional to the heating of the medium under shock conditions. For this reason we have computed the effects of finite amplitudes on heating patterns as discussed below.

There are two qualitatively different finite amplitude effects on the beam patterns of sound sources. First, under certain conditions, the distribution of the intensity of the sound itself is changed because of relatively greater attenuation of the axial portion of the beam. This tends to “flatten” the beam pattern when the axial portion of the beam becomes a sawtooth wave (Muir and Carstensen, 1980; Carstensen *et al.*, 1980, Shooter *et al.*, 1974). Second and perhaps more important for this study, the “heating pattern” of the sound field can be sharpened when the shock parameter for the axial portion of the beam is between 1 and 3. This arises because the heating rate increases very rapidly as a function of intensity once shock formation begins. Thus the large axial intensities produce disproportionately greater heating rates than the lower intensities away from the axis. When the shock parameter is much greater than 3, the transaxial intensity distribution and the heating rates combine to make the heating pattern broader than it is at low source intensities. We treated the subject by measuring the transaxial intensity pattern of the transducer at low intensities and computing finite amplitude effects for off-axis field points as though they corresponded to proportionally lower source intensities than points on the axis. Examples of such computed heating patterns are shown in Fig. 10.

### F. Data processing

To relate the observed heating rate at 1.5 s to the initial heating rate of the medium at each experimental condition, a

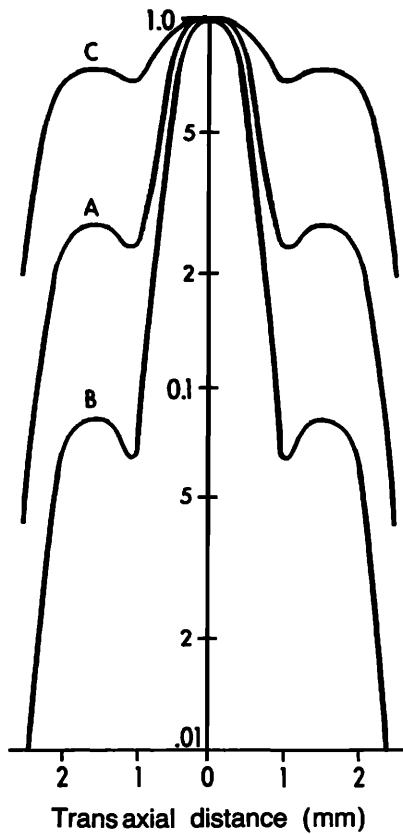


FIG. 10. Calculated nonlinear effects on heating patterns of focused sources. Frequency = 4 MHz,  $z_0 = 10$  cm;  $z_r = 2$  cm. All curves are normalized to axial heating rate. Curve A is for  $I_0 = 0.1$  W/cm<sup>2</sup> ( $\sigma = 0.24$ ); Curve B is for  $I_0 = 5$  W/cm<sup>2</sup> ( $\sigma = 1.7$ ); Curve C is for  $I_0 = 100$  W/cm<sup>2</sup> ( $\sigma = 7.5$ ). At low source intensities the heating pattern and the sound intensity beam pattern are identical. When  $\sigma = 1.7$ , the heating pattern is somewhat narrower than the small amplitude heating pattern but for very large axial intensities, when the field approaches saturation, the heating pattern actually becomes broader than the small amplitude pattern. Computations are based on the converging spherical wave model of the sound field.

normalized curve of axial temperature versus time was computed. We assume that the thermocouple junction is located on the axis of a radially symmetric heating pattern. The heating pattern can be modeled as a series of discrete coaxial rings about the thermocouple junction which is located on the axis of symmetry at  $r = 0, z = 0$  (see Fig. 11). The temperature at the origin from an instantaneous, ring, heat

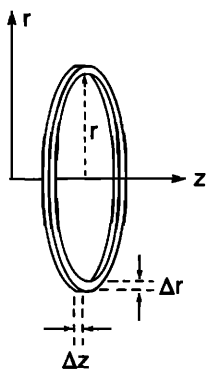


FIG. 11. The coordinate system used in modeling the heating pattern as a series of discrete coaxial rings distributed in  $r$  and  $z$ . Sound propagation is in the  $z$  direction with the  $z$  axis of the coordinate system coincident with the axis of the sound beam.

source  $Q [Q = 2\pi r \Delta r \Delta z T(r, z)]$  of cross section  $\Delta r \Delta z$  located at  $r, z$  is (Carslaw and Jaeger, 1959; Carstensen *et al.*, 1981)

$$T(t) = \frac{2\pi r \Delta r \Delta z T(r, z)}{8(\pi \kappa t)^{3/2}} \exp[-(r^2 + z^2)/4\kappa t], \quad (26)$$

where  $t$  is time and  $\kappa$  is the thermal diffusivity of the medium. The temperature at the origin from an arbitrary ultrasonically created heating pattern can be obtained by summation of an appropriate series of rings

$$T(t) = \sum_{\text{all } r} \sum_{\text{all } z} \left( \frac{\pi \Delta r \Delta z}{4} \right) \times \left[ \frac{r T(r, z)}{(\pi \kappa t)^{3/2}} \exp\left(-\frac{(r^2 + z^2)}{4\kappa t}\right) \right]. \quad (27)$$

The source strength  $T(r, z)$  is

$$T(r, z) = \frac{2(\alpha_{ws} + \alpha_{mat}) I(r, z) \Delta t}{\rho C}, \quad (28)$$

where  $I(r, z)$  is the local intensity,  $\rho$  is the density,  $C$  is the specific heat (mechanical units) of the medium, and  $\Delta t$  is the infinitesimal of time. Of course, because the propagation is nonlinear, both  $\alpha_{ws}$  and  $\alpha_{mat}$  are functions of  $r$  and  $z$ . In practice, the product  $2(\alpha_{ws} + \alpha_{mat}) I(r, z)$  was calculated as discussed above for the heating patterns. For a finite exposure period (e.g., 1.5 s) Eq. (28) is substituted in Eq. (26) and the summation (integration) carried out over  $r, z$ , and  $t$ . These plots provide a ratio between the rate of change of temperature observed at 1.5 s, when the effects of localized heating of the thermocouple are negligible, to the rate of heating of the medium,  $dT/dt$  at  $t = 0$ . Because of finite amplitude effects, a different heating pattern and diffusion correction was required for each new intensity in the experimental procedure.

In summary, the finite amplitude theory was used twice in these tests. Its primary use was to predict local heating rates as a function of source intensity. Secondarily, theory was used in the computation of the spatial heating patterns which, in turn, were used to compute the heat diffusion needed to relate the rate of rise of temperature at 1.5 s to the heating rate. In this way temperature measurements could be related to source intensity measurements through theory.

### III. EXPERIMENTAL TESTS

The raw temperature versus time data frequently provide a clear illustration of finite amplitude effects on heating. Figure 12 shows the temperature curves for two exposure conditions of equal average intensity. Curve A was a pulsed exposure with a source intensity of 15 W/cm<sup>2</sup> ( $\sigma$  approximately 3) during the on-time of the pulse, and with an average intensity of 0.25 W/cm<sup>2</sup>. Curve B was a continuous wave exposure with an intensity of 0.25 W/cm<sup>2</sup>. If the heating mechanism were linear, the two curves would be identical. However, the heating rate for case A was approximately three times that for case B. The experimental data in this form qualitatively demonstrate the increase in heating due to nonlinearities.

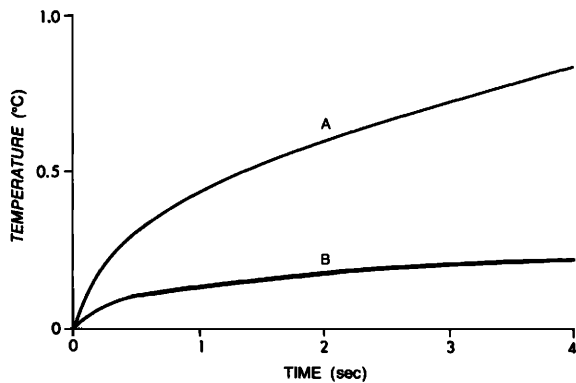


FIG. 12. Raw temperature data demonstrating nonlinear heating. In both examples, the temporal average source intensity is  $0.25 \text{ W/cm}^2$ . Curve B is c.w., whereas, in Curve A the waveform consists of a train of  $100 \mu\text{s}$  pulses each with a source intensity of  $15 \text{ W/cm}^2$ .

Figure 13 presents the normalized heating rates ( $H/I_0$ ) for a 4-MHz source with a focal length of 10 cm at positions in the sound field where  $z_r/z_0$  is 0.1 and 0.25. These observations are compared to the predictions of the focused [Eq. (21)] and spherically converging [Eq. (20)] models for the sound field. For  $z_r/z_0 = 0.25$ , both models are good predictors of nonlinear heating. For  $z_r/z_0 = 0.1$  the focused model continues to be a good predictor. However, as the focus is approached, the simplified spherically converging model, which ignores diffraction and hence leads to a narrower beam than is realized in practice, significantly overestimates the heating at all source intensities. Nevertheless, the experimental data illustrate the predicted characteristic that, as

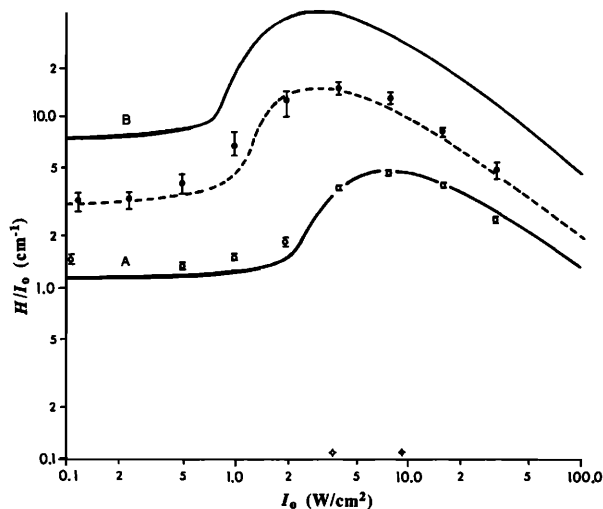


FIG. 13. Comparison of observed and predicted, normalized, heating rates showing the effect of proximity of the point of observation to the focus. Frequency = 4 MHz; thermocouple depth = 0.5 cm in 3% agar;  $z_0 = 10$  cm. Open circles,  $z_r/z_0 = 0.25$ ; solid circles,  $z_r/z_0 = 0.1$ . Curve A is the predicted heating for the  $z_r/z_0 = 0.25$  case using either the spherically converging wave or the focused wave models. Curve B shows that the spherically converging wave model (solid line) overestimates the heating rate at  $z_r/z_0 = 0.1$ . However, the focused wave model (dashed line) with the experimentally observed focal gain of  $G = 8.8$  satisfactorily predicts the heating at this distance. ( $\sigma = 2$  at  $\blacklozenge$  for curve A;  $\sigma = 2$  at  $\blacklozenge$  for curve B).

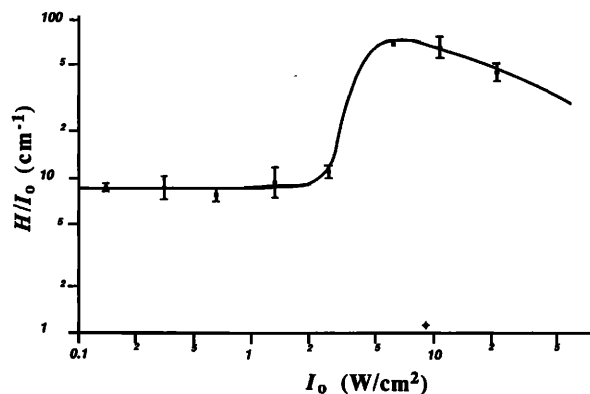


FIG. 14. Focal heating in a sharply focused sound field. Observed and predicted, normalized, heating rates are compared at the focus of a 3.6-MHz source with a focal length of 4.7 cm;  $G = 11$ ; thermocouple depth = 0.5 cm in 3% agar. Although the frequencies in Figs. 13 and 14 are roughly the same, the maximum weak shock heating is greater here because of the smaller focal length. Focused wave formulations were used for heating rate predictions. ( $\sigma = 2$  at  $\blacklozenge$ ).

the focus is approached, the nonlinear heating increases and the onset of this nonlinear heating occurs at lower source intensities [Fig. 6(b)].

The increase in finite amplitude heating with decreasing focal length  $z_0$  as anticipated in Fig. 6(c) is shown in Fig. 14. The transducer used for this test had approximately the same frequency (3.6 MHz) as in Fig. 13 but only one-half the focal length ( $z_0 = 4.7$  cm). Note that, in this example, the maximum heating rate exceeds by a factor of 10 that which would be expected if the mechanism were linear. In this case, the thermocouple was placed at the focus of the sound field. The solid curve is the predicted heating rate normalized to the source intensity using the focused model [Eqs. (5), (12), and (21)].

As noted in Fig. 6(a), increasing the frequency lowers the source intensity at which finite amplitude heating be-

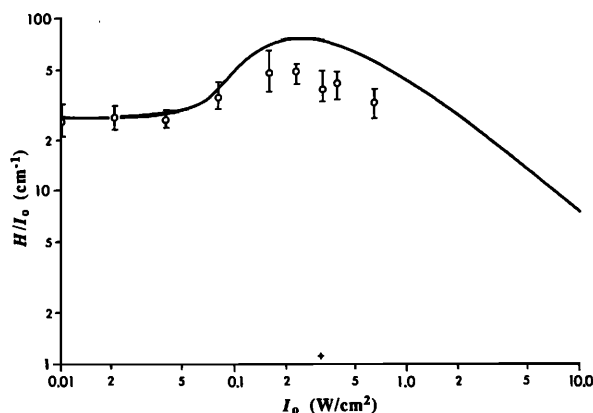


FIG. 15. Comparison of observed and predicted normalized, heating rates at 6 MHz. Thermocouple depth = 0.5 cm in 3% agar;  $z_0 = 18$  cm;  $z_r = 1.2$  cm. In comparison with Figs. 13 and 14, the higher frequency here results in a higher small signal heating rate. This tends to obscure the nonlinear contributions to the heating. In addition, the larger focal length used in these measurements tends to minimize the relative contributions of weak shock heating. ( $\sigma = 2$  at  $\blacklozenge$ ).

comes evident but this does not increase the magnitude of the finite amplitude losses. The small-signal absorption coefficient of materials do increase with frequency, however, and, hence, the finite amplitude losses tend to be obscured at higher frequencies. This is illustrated by comparison of the 6-MHz data in Fig. 15 with that for lower frequencies. A further reason for the lower heating elevation for the measured data in Fig. 15 is the fact that the attenuation in water is sufficiently high that we are at the limits of the applicability of weak shock theory.

#### IV. DISCUSSION

In general, nonlinear processes increase losses and heating. This results from the continuous distortion of the waveform and consequent generation of high frequency components in the wave as it progresses through the medium. The nonlinearly generated, high frequencies are absorbed more rapidly than the low frequency which characterizes the source field. The losses associated with the shock front are essentially independent of the linear absorption coefficient of the medium as long as it is small. This is the special case considered by weak shock theory. We have chosen to explore the usefulness of its predictions because it demonstrates the fundamental physical processes which are involved in nonlinear ultrasonic heating.

To test the usefulness of weak shock theory in predicting finite amplitude absorption, measurements of heating in 3% agar samples, produced after propagation through a water path, were conducted for a variety of frequencies and degrees of focusing. Measurements were made in the prefocal and focal regions. The theory was used to predict the acoustic intensity in the converging sound field, the rate of dissipation of the ultrasonic energy throughout the field and deviations of the heating pattern from the acoustic beam pattern. In spite of the fact that the weak shock theory for spherical waves (Blackstock, 1972) does not consider diffraction effects and the inherent absorption of the medium, it can be used to predict finite amplitude absorption with reasonable accuracy in the proximal focal region before diffraction introduces an important limitation to the amplitude of the beam. With Bacon's (1984) formulation for diffraction, finite amplitude heating can be predicted with reasonable accuracy even at the focus. Although the Gaussian beam is not the same as the true beam, Bacon (1986) has shown that it can be successfully matched to the field of a focused piston source to predict nonlinear effects. By combining finite amplitude absorption with the excess absorption of harmonics as the wave passes into the material surrounding the thermocouple, we have been able to describe the dissipation of sound in focused nonlinear ultrasound fields where the small signal absorption is relatively small. Because finite amplitude absorption is much greater in focused than in unfocused fields, the evidence for weak shock absorption in the current series of experiments is somewhat clearer than our earlier study of nonlinear absorption phenomena (Carstensen *et al.*, 1982).

The theoretical procedures in this paper provide reasonable models for the nonlinear losses for the experimental

conditions of this study. In particular, the spherically converging model is a good predictor of nonlinear loss on-axis in the prefocal region before diffraction effects limit the wave amplitude, and by using a Gaussian beam the model becomes a reasonable predictor of nonlinear loss near and at the focus. Even the Gaussian model, though, does not account for the minima and maxima that occur in the prefocal region. This near field structure gives rise to spatial fluctuations in the heating pattern, but these fluctuations tend to be smoothed out by thermal conduction within the medium. Indeed, the agreement that has been obtained with the Gaussian theory suggests that this mechanism can be very effective, and it is therefore not always necessary to model the detailed structures of the field. The version of the Gaussian beam model used here does not model the phase of the wave, but it has nevertheless been shown to give good predictions of the harmonic amplitudes (Bacon, 1984). The predictions are expected to be reliable in the vicinity of the focus, which is where the heating effects are greatest. There are, therefore, important biomedical applications where these predictions are relevant, e.g., exposure of the fetus through a poorly attenuating window of urine and/or amniotic fluid (Bacon and Carstensen, 1990). At present, there is no analytical solution of the general problem of focused sound fields including the effects of diffraction, dispersion, and absorption. Comprehensive solutions to the general problem involve computationally intensive, step-by-step propagations of the wave from source to field point taking into account the distortion by nonlinearities and the losses which occur at each step (Bakhvalov *et al.*, 1978; Haran and Cook, 1983; Swindell, 1986; Hart and Hamilton, 1988; Bacon, 1989; Bacon and Baker, 1989; Christopher, 1990; Christopher and Parker, 1990).

Because of its simplicity, this approach to nonlinear absorption and heating has been helpful in understanding the fundamental physical phenomena involved in finite amplitude absorption. Of particular interest here is the prediction [Eq. (17)] that the weak shock contribution to the total absorption can be written as the product of a purely geometrical term and a term that depends only on the shock parameter  $\sigma$ . Our experimental tests were chosen to emphasize this weak shock component of the heating. For most medical applications of focused ultrasound where small signal tissue absorption coefficients are large and where a significant part of the sound path is in tissue, it would be wise to begin with a theoretical formulation which includes these tissue losses.

Even when the propagation path is mainly in tissue, it has been shown that significant extra heating due to nonlinear propagation can occur. For instance, Swindell (1985) predicted that it is possible to obtain approximately 50% enhancement of heating for propagation in tissue, which is similar to the enhancement measured by Hynynen (1987). Measurements of nonlinear losses in biological tissue using focused, 1-MHz ultrasound were also reported by Goss and Fry (1981) and Fry *et al.* (1989). Duck and Starritt (1989) measured the excess absorption of the fundamental by comparing measured pulse energies in water at high and low source powers for several axial positions.

Success in hyperthermia and thermal surgery frequently

depends upon being able to deposit heat selectively at depths somewhat below the surface of the body. If plane-wave ultrasound is used, the maximum heat development is usually at the surface of the body. With plane waves at finite amplitudes, surface heating, if anything, would be exaggerated. On purely linear considerations, it is frequently desirable to use focused fields for deep heating. The qualitative characteristics of finite amplitude heating which have been illustrated here suggest ways in which nonlinear phenomena may be employed to selectively increase the absorption parameters of tissue and thus increase heating in desired locations in the deep tissues (Swindell, 1985, Hynynen, 1987). Theoretical developments which adequately consider the effects of diffraction, dispersion, and absorption along the entire path of propagation will be necessary for this and other applications in medical ultrasound to be realized (Christopher, 1990; Christopher and Parker, 1990).

## V. CONCLUSION

This paper has developed a method for predicting the heating rate due to the absorption of focused ultrasound under conditions of nonlinear propagation. A particular advantage of the method is its simplicity, with results being expressed in analytical form. If the propagation path contains a significant amount of material with a low attenuation, then a shock can form and the effective absorption parameter can be high compared with that for soft tissue. Under the experimental conditions used here, at a frequency of about 4 MHz, the maximum absorption coefficient in 3% agar was in the range 0.3–0.8 Np/cm. The method could be incorporated into a model of heat diffusion and perfusion to calculate temperature rises in applications such as hyperthermia or ultrasound diagnosis.

## ACKNOWLEDGMENTS

The authors are indebted to Professor Tom Muir, University of Texas at Austin, for his guidance in the early stages of this work and, in particular, to Professor David Blackstock, University of Texas at Austin and Visiting Scientist of the Rochester Center for Biomedical Ultrasound for many helpful discussions and comments on this manuscript. This work was supported in part by U.S.P.H.S. Grants No. GM09933 and CA39241.

## APPENDIX

The second-order, nonlinear, parabolic wave equation has a low-amplitude solution (e.g., Bacon, 1986)

$$p = \frac{p_0}{(1-jR)} e^{[-r^2/a^2(1-jR)] + j(\omega t - kz)} \quad (A1)$$

for a Gaussian beam with focus at  $z_f = 0$  and radial position  $r$ , where  $R = 2(z - z_0)/ka^2$ ,  $z_0$  is the focal length,  $a$  is the focal beam radius at the  $\exp(-1)$  amplitude level, and  $k$  is the wave number. The particle velocity can be determined from Eq. (A1) using  $u = \nabla\Phi$  where  $\Phi = -p/(j\omega\rho_0)$ . In cylindrical coordinates, this gives

$$u = \Phi \left( \frac{-2r}{a^2(1-jR)} \right) e_r + \Phi \left( \frac{-2jr^2}{ka^4(1-jR)^2} - jk + \frac{2j}{ka^2(1-jR)} \right) e_z. \quad (A2)$$

The intensity expressed as  $I = (1/2)\text{Re}(u \cdot p^*)$  becomes

$$I(z,r) = I_0 G^2 e^{[-2r^2/a^2(1+R^2)]} \left( \frac{rR}{r_0(1+R^2)^2} e_r + \frac{1}{(1+R^2)} e_z \right), \quad (A3)$$

where  $r_0 = ka^2/2$  and  $G$  is the amplitude gain at the focus. For this lossless case, the divergence of the intensity as given in Eq. (A3) is zero.

For the general nonlinear case, all of the harmonic amplitudes have the general form given by Eq. (A3) (Bacon, 1986) and hence it can be shown by integrating along a ray tube that the intensity is

$$I(z,r) = I_0 G^2 e^{[-2r^2/a^2(1+R^2)]} \left( \frac{rR}{r_0(1+R^2)^2} e_r + \frac{1}{(1+R^2)} e_z \right) \sum_{n=1}^{\infty} B_n^2[\sigma(z,r)], \quad (A4)$$

where the nonlinear losses are accounted for in the summation term and the Gaussian radial dependence of the shock parameter is described as

$$\sigma = \frac{\beta\epsilon_0 k z_0 G_f}{\sqrt{G_f^2 - 1}} \{ \ln[G_f + \sqrt{G_f^2 - 1}] + \ln[R + \sqrt{1 + R^2}] \} e^{[-r^2/a^2(1+R^2)]}. \quad (A5)$$

The divergence of Eq. (A4) gives the off-axis variation of the heating rate, i.e., the heating pattern as a function of the shock parameter

$$\nabla \cdot I(z,r) = I_0 \frac{\beta\epsilon_0 k G^2 G_f}{(1+R^2)^{3/2}} e^{[-3r^2/a^2(1+R^2)]} \times \frac{\partial}{\partial\sigma} \sum_{n=1}^{\infty} B_n^2[\sigma(z,r)]. \quad (A6)$$

The finite amplitude absorption for the focused case is obtained by using Eqs. (A6) and (A4) in Eq. (1) to give Eq. (17) where now

$$F = \frac{z_0 \sqrt{1+R^2}}{\sqrt{G_f^2 - 1}} \{ \ln[G_f + \sqrt{G_f^2 - 1}] + \ln[R + \sqrt{1+R^2}] \} \sqrt{1 + \left( \frac{rR}{r_0(1+R^2)} \right)^2}. \quad (A7)$$

For the cases described in this paper [ $rR/r_0(1+R^2)$ ] is small and  $F$  is given by Eq. (21).

- Bacon, D. R. (1984). "Finite amplitude distortion of the pulsed fields used in diagnostic ultrasound," *Ultrasound Med. Biol.* **10**, 189–195.  
 Bacon, D. R. (1986). "Nonlinear propagation in ultrasonic beams," PhD thesis, University of Bath, United Kingdom.  
 Bacon, D. R. (1989). "Prediction of *in situ* exposure to ultrasound: An improved method," *Ultrasound Med. Biol.* **15**, 355–361.

- Bacon, D. R., and Baker, A. C. (1989). "Comparison of two theoretical models for predicting non-linear propagation in medical ultrasound fields," *Phys. Med. Biol.* **34**, 1633–1643.
- Bacon, D. R., and Carstensen, E. L. (1990). "Increased heating by diagnostic ultrasound due to nonlinear propagation," *J. Acoust. Soc. Am.* **88**, 26–34.
- Bakhvalov, N. S., Zhileikin, Ya. M., Zabolotskaya, E. A., and Khoklov, R. V. (1978). "Focused high-amplitude sound beams," *Sov. Phys. Acoust.* **24**, 10–15.
- Blackstock, D. T. (1966). "Connection between the Fay and Fubini solution for plane sound waves of finite amplitude," *J. Acoust. Soc. Am.* **39**, 1019–1026.
- Blackstock, D. T. (1972). "Nonlinear acoustics (theoretical)," in *American Institute of Physics Handbook*, edited by D. E. Gray (McGraw-Hill, New York), pp. 3-183–3-205.
- Blackstock, D. T. (1991). "On the absorption of finite amplitude sound," *J. Acoust. Soc. Am.* (to be published).
- Carslaw, H. S., and Jaeger, J. C. (1959). *Conduction of Heat in Solids* (Clarendon, Oxford).
- Carstensen, E. L., Law, W. K., McKay, N. D., and Muir, T. G. (1980). "Demonstration of nonlinear acoustic effects at biomedical frequencies and intensities," *Ultrasound Med. Biol.* **6**, 359–368.
- Carstensen, E. L., Becroft, S. A., Law, W. K., and Barbee, D. B. (1981). "Finite amplitude effects on the thresholds for lesion production in tissues by unfocused ultrasound," *J. Acoust. Soc. Am.* **70**, 302–309.
- Carstensen, E. L., McKay, N. D., Dalecki, D., and Muir, T. G. (1982). "Absorption of finite amplitude ultrasound in tissues," *Acustica* **51**, 116–123.
- Christopher, P. T., and Parker, K. J. (1990). "Linear and nonlinear acoustic field propagation for medical devices," *IBM J. Supercomput.* (in press).
- Christopher, P. T. (1990). "Developments in shock wave propagation using the frequency domain solution to Burgers' equation," *J. Acoust. Soc. Am.* (submitted).
- Dickinson, R. J. (1985). "Thermal conduction errors of manganin-constantan thermocouple arrays," *Phys. Med. Biol.* **30**, 445–453.
- Duck, F. A., and Starritt, H. C. (1989). "The spatial distribution of excess absorption in water due to shock transmission," *Phys. Med. Biol.* **34**, 1623–1631.
- Fry, F. J., Dines, K. A., Reilly, C. R., and Goss, S. A. (1989). "Losses in tissue associated with finite amplitude ultrasound transmission," *Ultrasound Med. Biol.* **15**, 481–497.
- Fry, W. J., and Fry, R. B. (1954). "Determination of absolute sound levels and acoustic absorption coefficients by thermocouple probes—Experiment," *J. Acoust. Soc. Am.* **26**, 311–317.
- Goss, S. A., and Fry, F. J. (1981). "Nonlinear acoustic behavior in focused ultrasonic fields: Observations of intensity-dependent absorption in biological tissue," *IEEE Trans. Sonics Ultrason.* **SU-28**, 22–26.
- Haran, M. E., and Cook, B. D. (1983). "Distortion of finite amplitude ultrasound in lossy media," *J. Acoust. Soc. Am.* **73**, 774–779.
- Hart, T. S., and Hamilton, M. F. (1988). "Nonlinear effects in focused sound beams," *J. Acoust. Soc. Am.* **84**, 1488–1496.
- Hynynen, K. (1987). "Demonstration of enhanced temperature elevation due to nonlinear propagation of focussed ultrasound in dog's thigh *in vivo*," *Ultrasound Med. Biol.* **13**, 85–91.
- Lighthill, M. J. (1956). "Viscosity effects in sound waves of finite amplitude," in *Surveys in Mechanics*, edited by G. K. Batchelor and R. M. Davies (Cambridge University, Cambridge), pp. 250–351.
- Muir, T. G., and Carstensen, E. L. (1980). "Prediction of nonlinear acoustic effects at biomedical frequencies and intensities," *Ultrasound Med. Biol.* **6**, 345–357.
- Shooter, J. A., Muir, T. G., and Blackstock, D. T. (1974). "Acoustic saturation of spherical waves in water," *J. Acoust. Soc. Am.* **55**, 54–62.
- Swindell, W. (1985). "A theoretical study of nonlinear effects with focused ultrasound in tissues: An 'acoustic Bragg peak,'" *Ultrasound Med. Biol.* **11**, 121–130.
- Swindell, W. (1986). "Nonlinear effects with focused ultrasound in tissues: An improved model," *Proc. Inst. Acoust.* **8**, 79–84.
- Taylor, G. I. (1910). "The conditions necessary for discontinuous motion in gases," *Proc. R. Soc. London, Ser. A* **84**, 371–377.